Deep ocean biogeochemistry of silicic acid and nitrate

J. L. Sarmiento,[1] J. Simeon,[1] A. Gnanadesikan,[2] N. Gruber,[3] R. M. Key,[1] and R. Schlitzer[4]

Received 15 March 2006; revised 31 October 2006; accepted 27 November 2006; published 17 March 2007.

[1] Observations of silicic acid and nitrate along the lower branch of the global conveyor belt circulation show that silicic acid accumulation by diatom opal dissolution occurs at 6.4 times the rate of nitrate addition by organic matter remineralization. The export of opal and organic matter from the surface ocean occurs at a Si:N mole ratio that is much smaller than this almost everywhere (cf. Sarmiento et al., 2004). The preferential increase of silicic acid over nitrate as the deep circulation progresses from the North Atlantic to the North Pacific is generally interpreted as requiring deep dissolution of opal together with shallow remineralization of organic matter (Broecker, 1991). However, Sarmiento et al. (2004) showed that the primary reason for the low silicic acid concentration of the upper ocean is that the waters feeding the main thermocline from the surface Southern Ocean are depleted in silicic acid relative to nitrate. By implication, the same Southern Ocean processes that deplete the silicic acid in the surface Southern Ocean must also be responsible for the enhanced silicic acid concentration of the deep ocean. We use observations and results from an updated version of the adjoint model of Schlitzer (2000) to confirm that this indeed the case.

Citation: Sarmiento, J. L., J. Simeon, A. Gnanadesikan, N. Gruber, R. M. Key, and R. Schlitzer (2007), Deep ocean biogeochemistry of silicic acid and nitrate, *Global Biogeochem. Cycles*, *21*, GB1S90, doi:10.1029/2006GB002720.

1. Introduction

[2] Our present understanding of the large-scale distribution of silicic acid and nitrate in the ocean has been strongly influenced by the conveyor belt circulation paradigm described by *Broecker* [1991] and illustrated schematically in Figures 1a and 1b. The lower branch of the conveyor forms in the North Atlantic, travels south to the Southern Ocean, and then north into the Indian and Pacific oceans. Water is gradually lost from the lower branch as it upwells into the upper ocean and joins the return flow of the conveyor belt circulation. The upwelling component of this circulation is essentially a one-dimensional process driven by downward mixing of buoyancy. The deep water that is lost to upwelling is resupplied by the deep conveyor branch and returned eventually to the North Atlantic by the upper conveyor branch.

[3] Over the past decade, a number of difficulties with the conveyor belt circulation paradigm have been identified, and a new meridional overturning circulation paradigm has begun to emerge. Among the most important of the difficulties is that purposeful tracer experiments such as those of *Ledwell et al.* [1993], and related studies of temperature microstructure, have demonstrated that vertical diffusivities in the main thermocline are about an order of magnitude too small to account for the flux of buoyancy required to drive the generalized upwelling envisioned by the *Broecker* [1991] conveyor belt paradigm. Model simulations with lower vertical diffusivities such as suggested by the observations strongly imply that without a high vertical diffusivity to drive widespread upwelling, the upwelling of deep water becomes confined primarily to the Southern Ocean [e.g., *Gnanadesikan et al.*, 2004, 2007; *Hallberg and Gnanadesikan*, 2007]. Analyses of observations such as the silicic acid and nitrate distribution study of *Sarmiento et al.* [2004] suggest that upwelling of deep water is indeed confined primarily to the Southern Ocean, but also including significant vertical mixing and/or upwelling in the North Pacific. However, other observational analyses, including some geostrophic inverse models, suggest that upwelling in the Southern Ocean is either very small or even negative, i.e., downwelling [e.g., *Sloyan and Rintoul*, 2001; *Talley et al.*, 2003].

[4] On the basis of the studies suggesting strong Southern Ocean upwelling as well as a contribution from the North Pacific, we depict in Figures 1c and 1d a revised view of the meridional overturning circulation that preserves the conveyor belt but confines almost all upwelling to the Southern Ocean and North Pacific. *Sarmiento et al.* [2004] explored the consequences of this new conveyor belt circulation paradigm for the distribution of nitrate and silicic acid in the main thermocline. Our goal here is to examine its consequences for the deep ocean distribution of these

[1]Program in Atmospheric and Ocean Sciences, Princeton University, Princeton, New Jersey, USA.
[2]Geophysical Fluid Dynamics Laboratory, Princeton, New Jersey, USA.
[3]Institute of Bigeochemistry and Pollutant Dynamics, ETH Zurich, Zurich, Switzerland.
[4]Alfred-Wegener-Institute, Bremerhaven, Germany.

0886-6236/07/2006GB002720$12.00

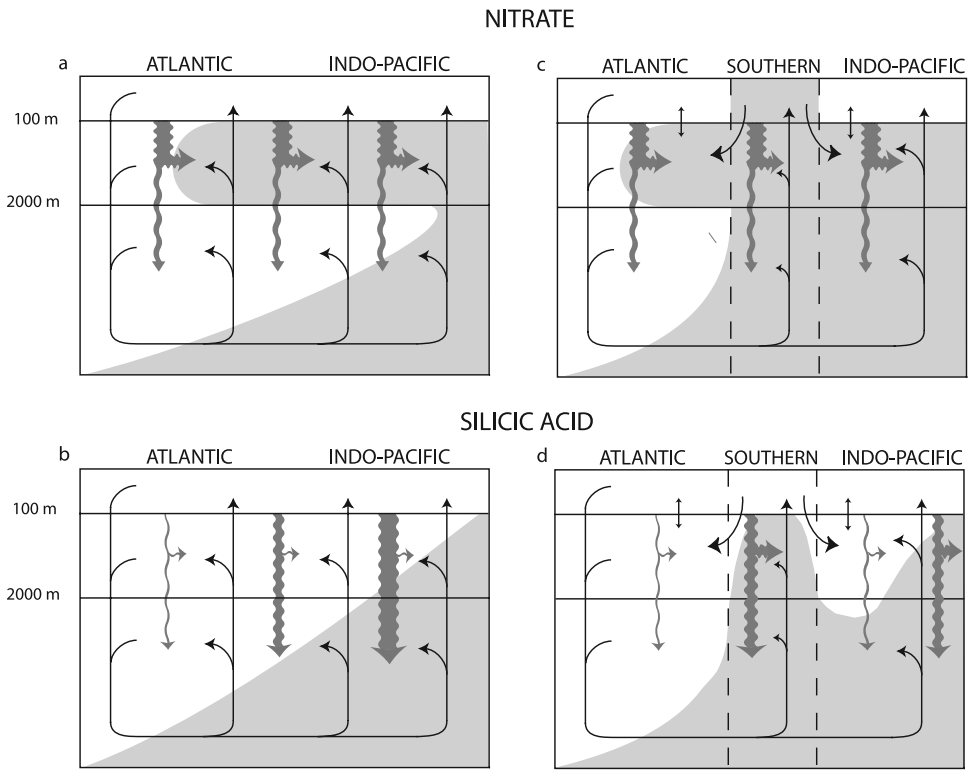

Figure 1. Contrasting conceptual models for what sets the global pattern of nitrate and silicic acid concentration in the world ocean. (a, b) Our interpretation of the *Broecker and Peng* [1982] model. (c, d) Our own view of the nitrate and silicic acid cycles.

tracers and to link this back to global patterns of organic nitrogen and opal export.

[5] Between the deep North Atlantic and deep North Pacific, opal dissolution leads to a silicic acid increase of $\sim$160 μmol kg^{-1} while organic matter remineralization leads to a nitrate increase of just $\sim$25 μmol kg^{-1} (see Figure 2). The resulting cumulative Si:N ratio of $\sim$6.4 is much greater than the Si:N uptake ratio of $\sim$1 that is typical of healthy diatoms living at the surface of the ocean [e.g., *Brzezinski*, 1985], or than the observed opal to organic matter Si:N export ratios, which are smaller than 1 almost everywhere except in the Southern Ocean and far north Indian and Pacific oceans [*Sarmiento et al.*, 2004]. On the basis of the circulation diagram of Figures 1a and 1b, *Broecker and Peng* [1982] long ago proposed that the high Si:N ratio of the deep ocean results from the vertical segregation of organic matter remineralization and opal dissolution. Organic matter remineralizes predominantly in the main thermocline while opal dissolves primarily in the deep ocean. When superimposed on the conveyor belt circulation, the vertical separation between organic matter remineralization and opal dissolution leads to a large accumulation of silicic acid and a more modest accumulation of nitrate along the pathway of the deep ocean branch of the conveyor belt (Figures 1a and 1b).

[6] The model of *Broecker and Peng* [1982] also has important consequences for the thermocline distribution of nitrate and silicic acid. They explain the silicic acid deficiency and high nitrate concentrations of the main thermocline (see Figure 2) primarily as resulting from the vertical separation between opal dissolution and organic matter remineralization. By contrast, *Sarmiento et al.* [2004] suggested that the thermocline properties are set not by the vertical separation of remineralization, but rather by the preformed nutrient concentrations of waters feeding into the main thermocline from surface waters of the Southern Ocean. Specifically, they suggested that the region that is of importance is where Subantarctic Mode Water (SAMW) forms from upwelled upper Circumpolar Deep Water. The SAMW subsequently spreads northward into the main thermocline of the entire Atlantic and most of the Indian Ocean as well as the southern hemisphere of the Pacific Ocean (see arrows with large heads in Figures 1c and 1d). The SAMW formation region is characterized by low iron concentrations and deep mixed layers that together lead to the growth of iron and/or light stressed diatoms with Si:N uptake ratios in excess of 1 [cf. *Hutchins and Bruland*, 1998; *Takeda*, 1998; *Franck et al.*, 2000; *Martin-Jezequel et al.*, 2000; *Watson et al.*, 2000; *Claquin et al.*, 2002; *Leynaert et al.*, 2004]. As a consequence, the surface water in the SAMW formation region becomes depleted in silicic acid while still retaining nitrate (see surface concentrations just north of 60°S in Figure 2). These properties are subsequently imparted to the main thermocline. These same processes lead to trapping of silicic acid in the deep Southern Ocean, which must eventually be exported as

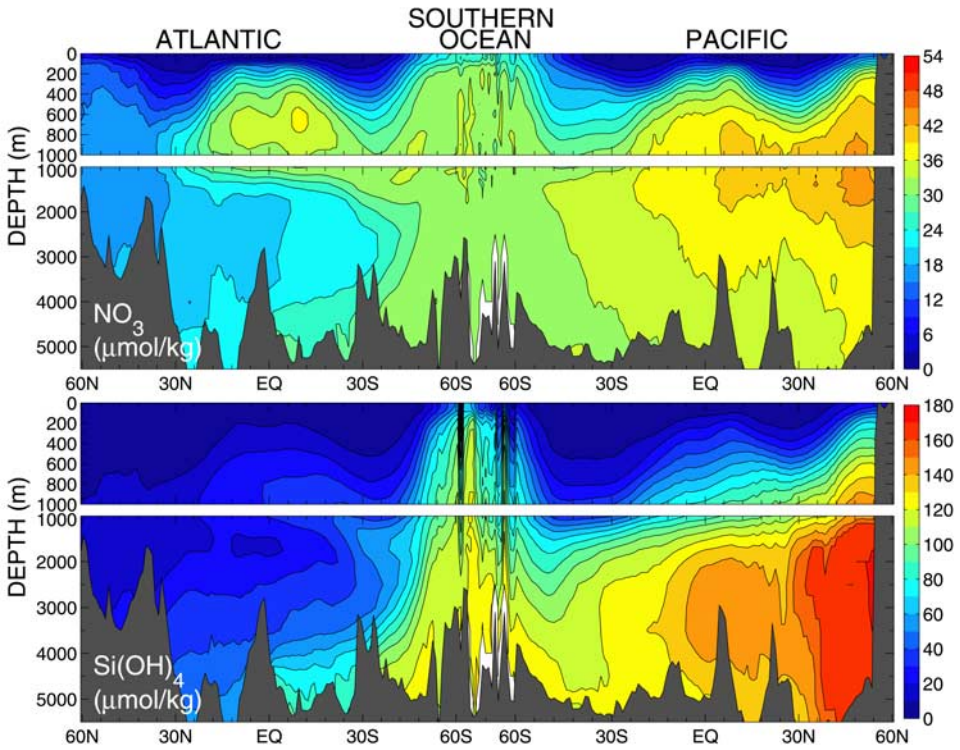

Figure 2. "Conveyor belt" sections of nitrate and silicic acid concentrations using the World Ocean Atlas 2001 [*Conkright et al.*, 2002]. The Atlantic and Pacific basins are zonal means. The Southern Ocean is represented by data at 60°S with a compressed length scale. Note the low silicic acid and high nitrate concentrations in the main thermocline.

Antarctic Bottom Water (AABW). The overall balance is maintained by having a low Si:N ratio in the SAMW and a high ratio in the AABW. The observational analysis of *Sarmiento et al.* [2004] shows that the North Pacific is the only major region of the ocean where thermocline properties appear to be strongly influenced by upwelling and/or mixing up of deep water rich in both silicic acid and nitrate, as in the old paradigm (see Figure 2).

[7] The *Sarmiento et al.* [2004] model has several major consequences for our understanding of global biogeochemistry. Those explored by them include the following. (1) The important role of nutrient injection into the main thermocline by SAMW in supporting about three quarters of the global biological production outside the Southern Ocean [cf. also *Marinov et al.*, 2006]. (2) The stripping out of silicic acid from upwelling Circumpolar Deep Water in the Southern Ocean. This gives both a high opal production within the Southern Ocean and a high Si:N ratio in the material that is exported out of the surface into the abyss in the Southern Ocean. By contrast, everywhere in the world that the SAMW influence is predominant has a low Si:N export ratio. This includes the entire Atlantic as well as most of the Indian Ocean and South Pacific [cf. *Sarmiento et al.* [2004]. (3) The silicic acid flux from the deep waters of the North Pacific into the main thermocline, which leads to a high opal to organic nitrogen production ratio throughout much of the North Pacific, including the tropics. The equatorial Pacific (and a portion of the Indian Ocean influenced by the Indonesian throughflow) is about as far south as the North Pacific silicic acid supply is able to advect before being lost to the abyss as opal.

[8] In this paper, we examine the implications of the *Sarmiento et al.* [2004] conceptual model for the distribution of silicic acid and nitrate in the deep ocean. If opal export to the deep ocean is indeed confined primarily to the Southern Ocean, with a significant contribution also from the tropical and North Pacific, we would expect that the silicic acid increase along the deep branch of the conveyor belt circulation would also be confined primarily to the Southern Ocean with an additional contribution from the tropical and North Pacific. By contrast, the abundant supply of nitrate (and phosphate) in the main thermocline, and the globally more evenly distributed export of organic matter that results from this, should lead to a more gradual increase in nitrate along the lower branch of the conveyor belt (though obviously with local variations in export influenced by where strong vertical exchange between the thermocline and surface ocean occurs).

[9] We use a sequence of approaches to examine the biogeochemistry of deep ocean silicic acid and nitrate. (1) We begin with maps of silicic acid and nitrate in the deep ocean as well as plots of silicic acid versus nitrate for a first identification of where the big silicic acid and nitrate increases occur in the deep ocean. (2) We estimate the fraction of silicic acid and nitrate that has been added by opal dissolution and organic matter remineralization for each

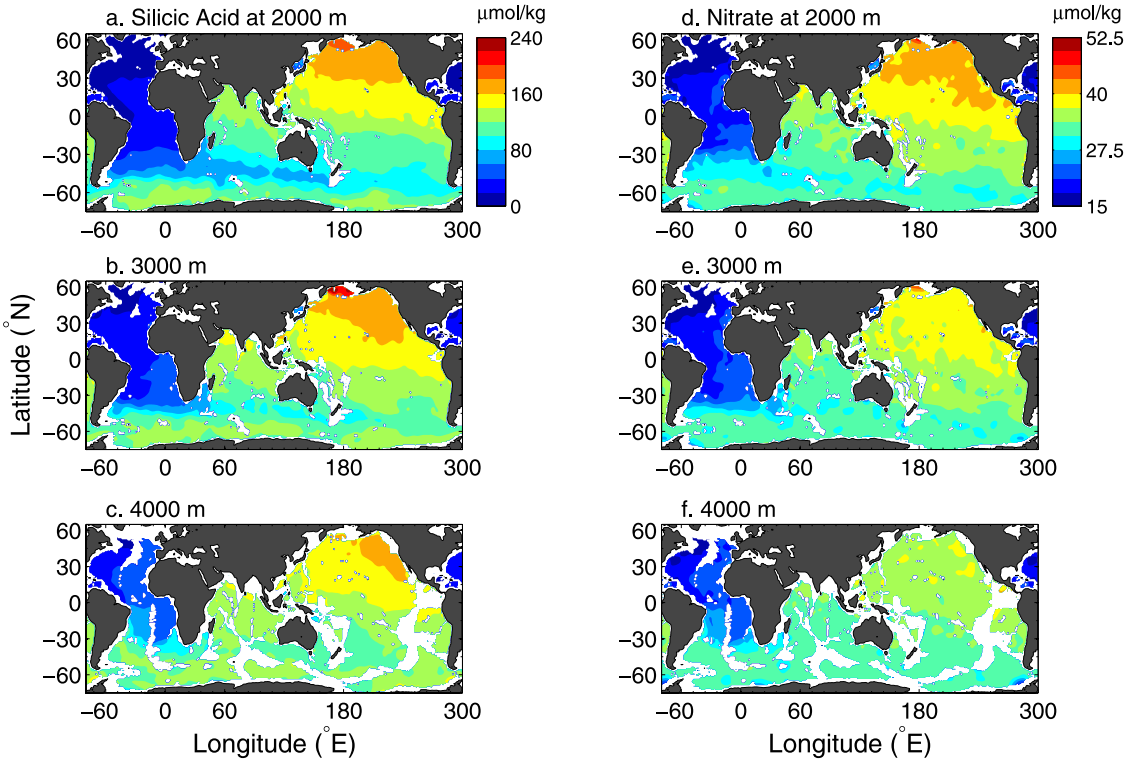

Figure 3. (a, b, c) Maps of silicic acid and (d, e, f) nitrate using World Ocean Atlas 2001. Depth levels from top to bottom are 2000 m, 3000 m, and 4000 m.

of the major ocean basins and the Southern Ocean. This analysis shows that the Southern Ocean is indeed the predominant region of opal dissolution, but that the North Pacific is also important. We further use radiocarbon to estimate the rate of opal dissolution and organic matter remineralization wherever the observations permit. (3) Finally, we analyze sediment trap observations and the adjoint model of *Schlitzer* [2000] to determine the extent to which the predominance of the Southern Ocean in the high Si:N ratio of deep waters can be attributed primarily to the preferential export of silicic acid in this region versus preferential dissolution of opal in deep waters in this region.

[10] All of the discrete data used in this study were taken from the GLODAP collection [*Key et al.*, 2004; *Sabine et al.*, 2005]. When it was necessary to determine bomb radiocarbon contamination, only those samples that had an estimated bomb ^{14}C contamination $\leq$5‰ were used. Maps and sections of nitrate and silicic acid are based on the World Ocean Atlas, 2001 [*Conkright et al.*, 2002] except those that require potential alkalinity, in which case maps and data from the GLODAP atlas are used.

2. Deep Distribution of Silicic Acid and Nitrate

[11] We choose 2000 m as a nominal depth horizon for the top of the deep water in our analysis. Figure 3 shows maps of silicic acid and nitrate at 2000 m and also at 3000 and 4000 m, below which the increasing topography makes it more difficult to distinguish the tracer patterns. The color scales have been set such that the ratio of the range for Si to that for N is approximately equal to the mean overall ratio of Si:N addition to the deep ocean of 6.4. The overall pattern of both the silicic acid and nitrate on all three of these depth levels is the large increase in concentration along the deep branch of the conveyor belt circulation from the North Atlantic to the northern Indian and Pacific oceans. The pattern of the two tracers is nearly identical, but there are subtle differences that illustrate the contrasting behavior of silicic acid and nitrate, and which shall show up better in later analysis. These include: (1) that the low silicic acid concentrations of the Atlantic Ocean persist much farther to the south than the low nitrate concentrations indicating a smaller addition of silicic acid relative to nitrate; (2) the striking tongue of extremely low silicic acid North Atlantic Deep Water (NADW) that flows into the Southern Ocean from the Atlantic and then to the east around the Southern Ocean (a similar feature can be seen in the salinity distribution owing to the relatively high salinity of NADW relative to Circumpolar Deep Water, CDW), as contrasted with nitrate for which the NADW signature in the Southern Ocean, while present, has a smaller contrast with the surrounding waters to both the north and south; (3) the large increase of silicic acid concentration toward the south against the Antarctic continent, with a more modest corresponding nitrate signal; and (4) the tendency for the increase of silicic acid in the Pacific to have a stronger relative gradient in the tropical and North Pacific than for nitrate, which tends to have a more gradual increase across the entire Pacific. These observations are all consistent with a relatively uniform source of nitrate to the deep ocean, with

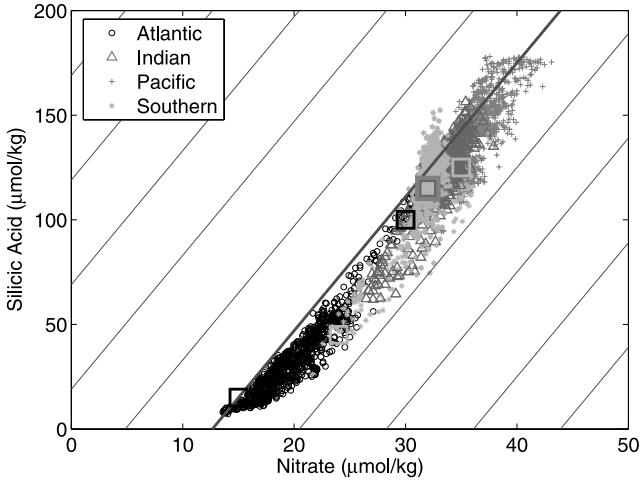

Figure 4. Scatter plot of silicic acid versus nitrate with contour lines of $Si^*_{deep} = [Si(OH)_4] - 6.4 \cdot [NO_3^-] + 81$. The thicker gray contour is for $Si^*_{deep} = 0$. The values of Si^*_{deep} are positive to the left and negative to the right of the zero contour. Data shown are from GLODAP discrete samples that have radiocarbon measurements.

silicic acid being added preferentially in the Southern Ocean as well as in the tropical and North Pacific.

[12] In an attempt to better discern the relationship between the addition of silicic acid and the addition of nitrate to the deep ocean, we show in Figure 4 a scatter plot of silicic acid versus nitrate for all data below 2000 m. Lines are included with a Si:N slope of 6.4. The thicker gray line goes through our best estimate of the properties of NADW in the North Atlantic. Specific features from this plot that further illustrate the contrasting behavior of silicic acid and nitrate include the following. (1) A somewhat lower Si:N slope in the Atlantic Ocean data than for other basins. This implies a low Si:N ratio in opal dissolution and organic matter remineralization occurring in this basin, but the overall signal of local dissolution and remineralization processes is obscured by mixing between the NADW and AABW end-members. (2) A higher Si:N slope of the Southern Ocean data. This is consistent with the high ratio of opal dissolution to organic matter required by our hypothesis, but again the signal is partially obscured by mixing between the various water mass end-members in the Southern Ocean, which include NADW and AABW, as well as the deep water return flows of both the Indian and Pacific oceans. (3) Intermediate Si:N slopes in the Indian and Pacific oceans which indicates preferential opal dissolution in those basins relative to the Atlantic.

[13] Our analysis of Figure 4 motivates defining a tracer $Si^*_{deep} = [Si(OH)_4] - 6.4 \cdot [NO_3^-] + 81$ that we can map on depth surfaces. The Si:N slope of 6.4 is the deep ocean ratio of opal dissolution to organic nitrogen remineralization that we gave earlier based on the cumulative silicic acid and nitrate increase between the North Atlantic and North Pacific. The constant of 81 μmol kg^{-1} fixes Si^*_{deep} to 0 in the North Atlantic. This tracer will remain constant if opal dissolution and organic matter remineralization occur at the mean ratio of 6.4. It will decrease if nitrate is added preferentially, i.e., with Si:N < 6.4 (as in the Atlantic and South Indian and Pacific oceans, per our model) and increase if silicic acid is added preferentially, i.e., with Si:N > 6.4 (as in the Southern Ocean and North Pacific, per our conceptual model).

[14] Figure 5 shows Si^*_{deep} at a depth of 2000, 3000, and 4000 m. At a depth of 2000 m, the Si^*_{deep} concentration of the NADW drops rapidly from its initial value of 0 μmol kg^{-1} to concentrations of -20 μmol kg^{-1} and lower as nitrate gets added to the water with little or no silicic acid. Water below 2000 m in the Atlantic has higher Si^*_{deep} due primarily to the influence of Antarctic Bottom Water coming in from the south. A particularly dramatic feature that we also saw in the silicic acid data of Figure 3 is the influence of the low Si^*_{deep} NADW as it flows around the Southern Ocean, particularly at a depth of 2000 m.

[15] The high Si:N signature of the opal dissolution and organic matter remineralization in the deep Southern Ocean is clearly evident at all three depth levels banked up against the Antarctic continent. In interpreting these observations, one must have in mind that isopycnal surfaces slope sharply up toward the surface in this region. Thus the observations farther to the south at a depth of 2000 and 3000 m, as well as more generally over all of the 4000 m depth surface, correspond to deeper water masses such as the upwelling CDW, and the water masses that go to form the AABW; whereas the observations farther to the north, particularly at 2000 and 3000 m, are strongly influenced by deep water outflows from all three ocean basins.

[16] Within the Southern Ocean, Si^*_{deep} attains values of 20 μmol kg^{-1} and higher. At 2000 and 3000 m depth, this high Si^*_{deep} CDW and AABW water is isolated from the rest of the ocean, but at a depth of 4000 m, we see that it feeds into all three ocean basins, most notably in the Indian and Pacific oceans. Within the Southern Ocean, the concentration of Si^*_{deep} drops initially toward the north owing to the influence of NADW, but then changes little within the Atlantic, and South Indian and Pacific oceans. It is only when the deep conveyor circulation reaches the North Pacific, that Si^*_{deep} increases to values as high as 40 μmol kg^{-1}. The Indian Ocean also has some regions of elevated values.

[17] We thus see that the distribution of Si^*_{deep} suggests a low ratio of opal dissolution to organic matter remineralization in the deep Atlantic Ocean, a high ratio in the Southern Ocean and North Pacific, and an average ratio in other regions. However, this analysis is of somewhat limited utility because it does not differentiate very well between concentration changes owing to mixing (e.g., between NADW and AABW in the Atlantic Ocean) from those due to in situ opal dissolution and organic matter remineralization. For this, we turn to a discussion of the silicic acid and nitrate anomaly distributions.

3. Silicic Acid and Nitrate Anomaly Distributions

[18] We are interested in estimating the in situ silicic acid and nitrate concentration increases owing to opal dissolution and organic matter remineralization in various basins of

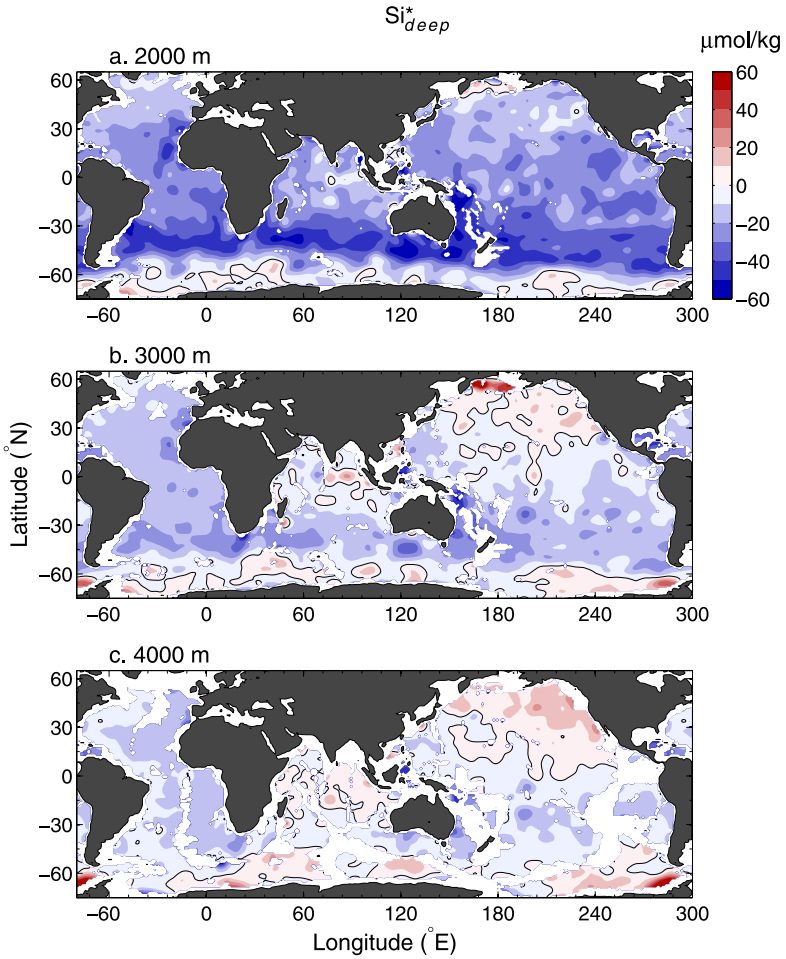

Figure 5. Deep Si* in μmol kg^{-1} defined as $Si^*_{deep} = [Si(OH)_4] - 6.4 \cdot [NO_3^-] + 81$ based on the maps of *Conkright et al.* [2002].

the world ocean. To do so, we need to determine a background concentration that a water parcel would have if no silicic acid or nitrate had been added to it. The strategy we follow is analogous to that used by *Broecker et al.* [1991] in their examination of various properties in the deep Atlantic Ocean, where a conservative tracer is used to determine the fraction of NADW and AABW for a given water parcel. Using this information, and the NADW and AABW end-member concentrations, they determine the background concentration of a tracer C_{BKG}, which is due to conservative mixing. The difference between this background concentration and the observed concentration, C_{obs}, is the anomaly due to remineralization or dissolution, $\Delta C = C_{obs} - C_{BKG}$. We can also calculate the radiocarbon anomaly concentration and use this to obtain an age estimate, τ, from which we can estimate the dissolution or remineralization rate, $\Delta C/\tau$. We discuss next how we do this calculation for the Atlantic Ocean north of 35°S, the Indo-Pacific Ocean north of 35°S, and the Southern Ocean south of 35°S.

[19] Following *Broecker et al.* [1991], we use PO_4^* as a conservative tracer to determine the relative contribution of the NADW and AABW end-members to a given water parcel in the interior of the Atlantic. We define PO_4^* differently from *Broecker et al.* [1991] in that we use an oxygen to phosphate stoichiometric ratio of 170 [*Anderson and Sarmiento*, 1994] rather than 175,

$$PO_4^* = \left[PO_4^{3-}\right] + \frac{[O_2]}{170} - 1.95\ \mu\text{mol kg}^{-1}. \qquad (1)$$

Because we are interested in analyzing remineralization within the Atlantic Ocean, we choose a northern end-member concentration in the region between 40°N and 50°N (nominally 45°N), and a southern end-member concentration within the 40°S to 30°S band (nominally 35°S). From maps of PO_4^* on depth surfaces, we choose for AABW entering the Atlantic across 35°S a value of 1.40 μmol kg^{-1}, which corresponds to the concentration that one sees in the southwest corner off South America at a depth of ~4000 m. For NADW, we choose a value of 0.76 corresponding to what is seen in the deep North Atlantic. We can use this information to define a fraction of NADW that varies linearly from 0 to 1 as the PO_4^* concentration varies from 0.76 to 1.40 μmol kg^{-1}. The equation for the line is $(y_1 - y_0) = m(x_1 - x_0) + b$, where m is the slope and b is the y intercept. PO_4^* is the independent variable, x, and f_{NADW} is the

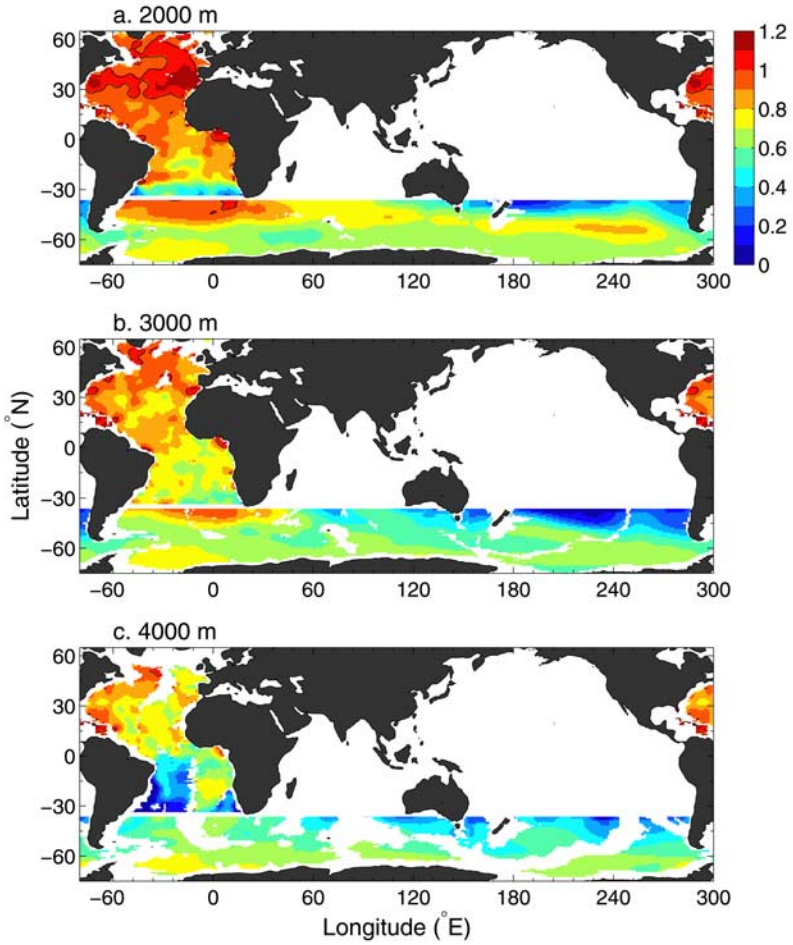

Figure 6. In the Atlantic Ocean north of 35°S, the fraction of NADW calculated relative to the region between 40°N and 50°N where f_{NADW} is set to 1.0, and the region between 40°S and 30°S, where f_{NADW} is set to 0. In the Southern Ocean south of 35°S, indicated by a thick white line in the South Atlantic, the fraction of the Atlantic end-member calculated relative to the Atlantic Ocean between 40°S and 30°S where $f_{ATL} = 1.0$, to the Indian and Pacific oceans between 40°S and 30°S where $f_{ATL} = 0$. See discussion in text for how these fractional contributions are estimated. Data source for the Atlantic is *Conkright et al.* [2002] and for the Southern Ocean it is *Key et al.* [2004] and *Sabine et al.* [2005]. The mismatch in topography at 35°S in the Atlantic is due to the difference in the topography in these two data sources.

dependent variable, y. For the end-members, we let $(x_0, y_0) = (1.4, 0)$ and $(x_1, y_1) = (0.76, 1)$. This gives $m = -1/(1.40 - 0.76)$ and $b = 0$, i.e.,

$$f_{NADW} = \frac{1.40 - PO_4^*}{1.40 - 0.76}. \quad (2)$$

Figure 6 shows the fraction of NADW at 2000, 3000, and 4000 m, from which we can confirm that its distribution goes from 1 in the North Atlantic to 0 at the southern boundary. The Mediterranean Sea Water (MSW) has values of $f_{NADW} > 1.0$ due to MSW having a lower PO_4^* than the other components of NADW, but the influence of this water is confined mostly to above 2000 m where it has minimal impact on our analysis.

[20] We consult the scatter plots of silicic acid, nitrate, and radiocarbon versus PO_4^* shown in Figures 7a, 7b, and 7c, in order to determine the NADW and AABW end-member concentrations. The NADW concentration of silicic acid and nitrate obtained in this way are both 15 μmol kg^{-1}. The AABW end-member entering the Atlantic at 35°S has silicic acid and nitrate concentrations of 100 μmol kg^{-1} and 30 μmol kg^{-1}, respectively. Radiocarbon has a concentration of −75‰ and −150‰ in the NADW and AABW, respectively. Boxes in Figures 7a, 7b, and 7c denote the end-member concentrations. This analysis gives the following equations for excess silicic acid due to dissolution of opal, excess nitrate due to remineralization of organic nitrogen, and radiocarbon deficit due to decay:

$$\begin{aligned} \Delta Si_{ATL} &= [Si(OH)_4] + 85 \cdot f_{NADW} - 100 \\ \Delta N_{ATL} &= [NO_3^-] + 15 \cdot f_{NADW} - 30 \\ \Delta(\Delta^{14}C)_{ATL} &= \Delta^{14}C - 75 \cdot f_{NADW} + 150 \end{aligned} \quad . \quad (3)$$

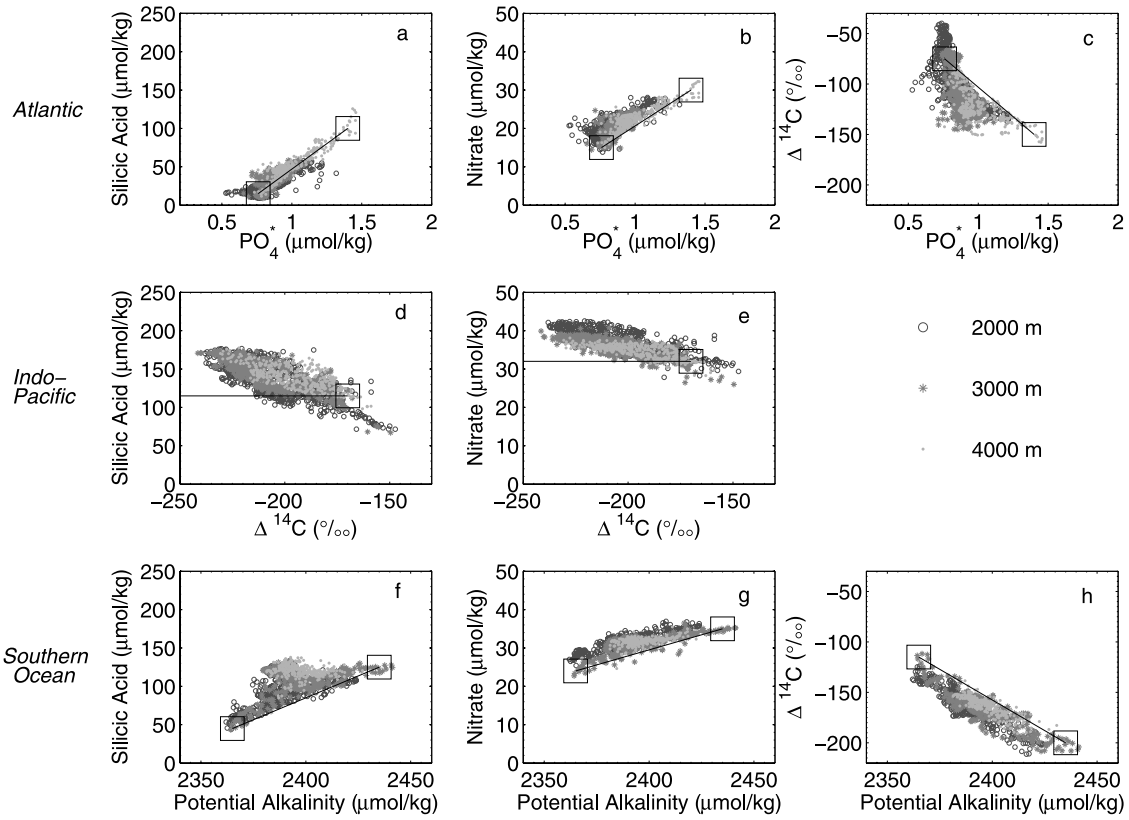

Figure 7. Scatter plots used for silicic acid, nitrate and radiocarbon end-member identification. (a, b, c) Atlantic Ocean observations plotted versus PO_4^*. (d, e) Indo-Pacific observations plotted versus radiocarbon. (f, g, h) Southern Ocean observations plotted versus potential alkalinity. The end-members concentrations are indicated by hollow black squares with a straight mixing line drawn between them. Data shown are from the World Ocean Atlas 2001 (silicic acid, nitrate, and PO_4^* [*Conkright et al.*, 2002]) and GLODAP Atlas 2004 (radiocarbon and alkalinity [*Key et al.*, 2004; *Sabine et al.*, 2005]). Only data from every five degrees (latitude and longitude) at depth levels 2000 m, 3000 m and 4000 m are shown, except for the Atlantic 4000 m depth level, where data from every two degrees are shown.

We can calculate the radiocarbon age from

$$\tau = -\ln\left[1 + \Delta\left(\Delta^{14}\mathrm{C}\right)/1000\right] \cdot 8033 \text{ yr}, \tag{4}$$

and the opal dissolution and organic nitrogen remineralization rates by dividing the age into the concentration change.

[21] From maps of radiocarbon on depth surfaces and by consulting Figures 7d and 7e, we find that the youngest water entering the Indian Ocean across 35°S at a depth of 2000 m occurs near Madagascar with a radiocarbon of −160‰. However, this water type is confined by the topography to the southwest corner of the basin. We thus choose as our CDW end-member at 35°S a source water farther to the east with an older radiocarbon of −170‰ (note that the radiocarbon measurement error is ∼4‰, and these values represent regional averages, so the difference between these alternatives is readily distinguishable). The youngest CDW entering the Pacific at 35°S occurs at a depth of ∼4000 m east of New Zealand also with a radiocarbon of about −170‰. The silicic acid concentrations that correspond to both the aforementioned Indian and Pacific Ocean radiocarbon end-members is 115 μmol kg^{-1}. Similarly, the nitrate concentrations are 32 μmol kg^{-1} in both basins. We thus treat the Indo-Pacific as a single basin with the following equations for excess silicic acid due to dissolution of opal, excess nitrate due to remineralization of organic nitrogen, and radiocarbon deficit due to decay [cf. *Mantyla and Reid*, 1995; *Reid*, 1997]:

$$\begin{aligned} \Delta \mathrm{Si}_{IP} &= \left[\mathrm{Si(OH)_4}\right] - 115 \\ \Delta \mathrm{N}_{IP} &= \left[\mathrm{NO_3^-}\right] - 32 \\ \Delta\left(\Delta^{14}\mathrm{C}\right)_{IP} &= \Delta^{14}\mathrm{C} + 170 \end{aligned} \quad . \tag{5}$$

As for the Atlantic, we can calculate a radiocarbon-based age and opal dissolution and organic nitrogen remineralization rates.

[22] Unmixing the Southern Ocean deep waters is much more challenging than for the other basins because there are at least four end-members: inflowing deep waters from the Atlantic, Indian, and Pacific oceans, and formation of

AABW from surface waters in the Antarctic. The following considerations allow us to simplify the problem:

3.1. Elimination of Antarctic End-Member

[23] In our conceptual model of the Southern Ocean, water upwells from the abyss into the Antarctic zone, and then either returns back to the abyss as AABW or flows out of the Antarctic into the Subantarctic and then into the main thermocline as SAMW and AAIW. As in the work of *Broecker and Peng* [1982], we assume that surface water in the Antarctic retains most of the properties of the CDW source except that it is cooled, freshened, and oxygenated. The lateral input of Subantarctic waters into the upper waters of the Antarctic zone will modify the Antarctic properties somewhat, but the impact of these on Antarctic Bottom Water properties does not appear to be large. In the case of silicic acid and nitrate, this means that we can treat the Antarctic box as if it were part of the CDW box, thus eliminating this end-member.

3.2. Combining the Indian and Pacific Ocean End-Members

[24] We assume that the Indian and Pacific Ocean deep waters entering the Southern Ocean have similar nitrate and silicic acid concentrations such that they can be represented by a single end-member concentration.

[25] With these simplifications we have the following equation for the background concentrations of silicic acid and nitrate:

$$C_d^{CDW})_{BKG} = f_{ATL} \cdot C_d^{ATL} + f_{IP} \cdot C_d^{IP}, \tag{6}$$

where *IP* refers to the Indo-Pacific, *ATL* to the Atlantic, *C* is concentration, and *f* is water mass fraction. Conservation of mass requires

$$f_{ATL} + f_{IP} = 1, \tag{7}$$

which allows us to simplify (6) to

$$C_d^{CDW})_{BKG} = f_{ATL} \cdot C_d^{ATL} + (1 - f_{ATL}) \cdot C_d^{IP}. \tag{8}$$

[26] By analogy with the Atlantic Ocean, we can solve this equation if we have one conservative tracer. We cannot use PO_4^* because it is modified by oxygenation in the surface Antarctic zone. Salinity is also modified in the surface Antarctic by freshening. Biogeochemical tracers in general will not be conserved in the CDW box because of the nonnegligible biological flux term. However, a biogeochemical tracer for which the biological flux appears to be small to negligible is potential alkalinity [*Brewer et al.*, 1975], which we define here without the usual salinity correction of 35/*S*,

$$P_{Alk} = Alk + [NO_3^-]. \tag{9}$$

The contribution of nitrate cycling to alkalinity is removed by adding nitrate concentration to the alkalinity, leaving only the influence of $CaCO_3$. The flux of $CaCO_3$ in the entire Southern Ocean is thought to be small to negligible (see extensive references in review by *Sarmiento et al.* [2002]).

[27] From Southern Ocean P_{Alk} data we estimate an Atlantic end-member concentration of 2365 μmol kg^{-1} entering the Southern Ocean across 35°S, and for the Indo-Pacific an end-member concentration of 2435 μmol kg^{-1}. This gives

$$f_{ATL} = \frac{2435 - P_{Alk}}{2435 - 2365}. \tag{10}$$

Figure 6 shows the fraction of Atlantic water at 2000, 3000, and 4000 m, from which we can see that its distribution does indeed go from 1 in the South Atlantic to 0 along the South Pacific Ocean at 35°S. Our assumption about the South Indian end-member being equal to the South Pacific end-member is not quite satisfied; the lowest Atlantic end-member concentration we see at 35°S in the Indian Ocean is about 0.2. We discuss the impact of this below.

[28] We consult the scatter diagrams of silicic acid and nitrate plotted against P_{Alk} shown in Figures 7f, 7g, and 7h to determine their end-member concentrations. We choose Atlantic and Indo-Pacific $Si(OH)_4$ end-member concentrations of 45 and 125 μmol kg^{-1}, respectively; for NO_3^-, we choose 24 and 35 μmol kg^{-1}, respectively; and for radiocarbon we choose −115‰ and −200‰, respectively. The final equations for the Southern Ocean are

$$\begin{aligned} \Delta Si_{SO} &= [Si(OH)_4] + 80 \cdot f_{ATL} - 125 \\ \Delta N_{SO} &= [NO_3^-] + 11 \cdot f_{ATL} - 35 \\ \Delta(\Delta^{14}C)_{SO} &= \Delta^{14}C - 85 \cdot f_{ATL} + 200 \end{aligned} \quad . \tag{11}$$

[29] The key features of the ΔSi distribution of Figure 8 are the large values of ΔSi in the Southern Ocean against the Antarctic continent, and in the North Pacific. In the Southern Ocean, ΔSi is defined relative to a value of 0 μmol kg^{-1} at 35°S in NADW in the South Atlantic and 0 μmol kg^{-1} in deep waters of the South Indian and Pacific oceans entering into the Southern Ocean. Thus the increase of ΔSi toward the south represents the cumulative effect of opal dissolution in the Southern Ocean adding silicic acid to the deep waters entering from all three ocean basins. In Figure 9, we see that the increase in ΔN is more gradual than for ΔSi, with significant increases in the eastern Atlantic where ΔSi hardly changes, and much less of an increase in the Southern Ocean.

[30] We noted earlier that f_{ATL} as defined by (10) drops only to ~0.2 instead of 0 in the southern Indian Ocean, indicating that the P_{Alk} end-member concentration for the Indian Ocean should be ~2421 μmol kg^{-1} rather than the nominal Indo-Pacific value of 2435 μmol kg^{-1} that we chose. We estimate that using the Indo-Pacific end-member for Indian Ocean water leads to an overestimate of ΔSi_{SO} by 0 to 9 μmol kg^{-1}, increasing linearly as the Indian Ocean contribution rises from 0 to 100%. Similarly, ΔN_{SO} will be overestimated by 0 to 0.7 μmol kg^{-1} as the Indian Ocean contribution increases from 0 to 100%. This is why Figures 8 and 9 show somewhat higher ΔSi and ΔN in

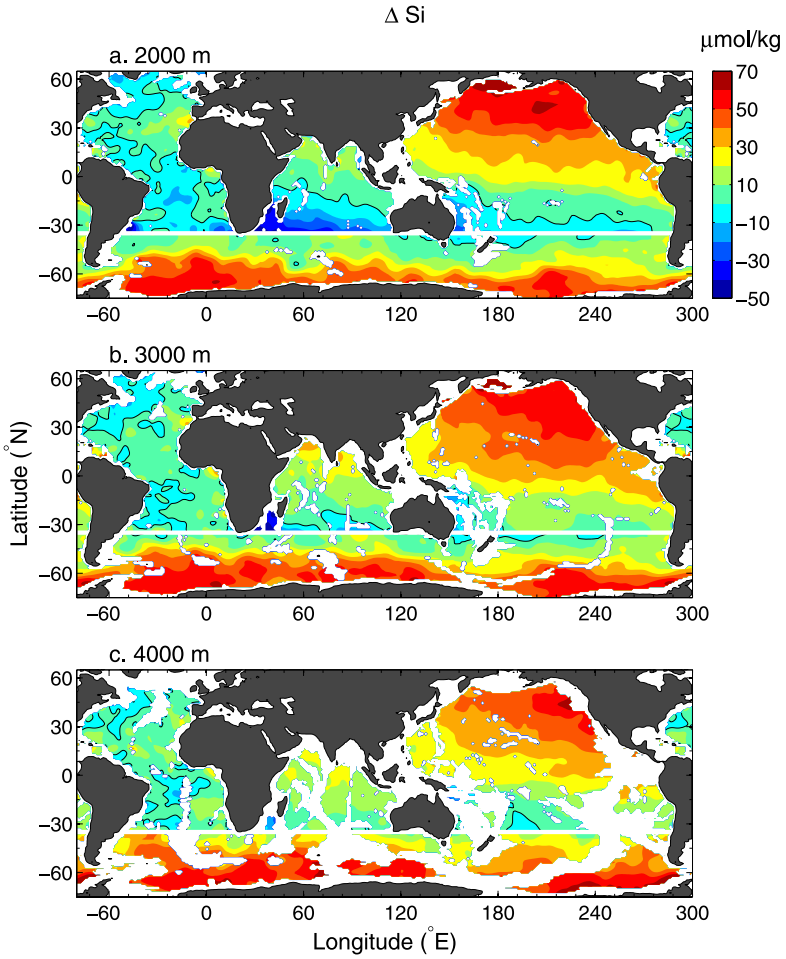

Figure 8. Global maps of ΔSi based on the World Ocean Atlas 2001 and GLODAP Atlas [*Conkright et al.*, 2002; *Key et al.*, 2004; *Sabine et al.*, 2005] and analyzed as described in the text. The analysis is performed separately for the Atlantic, Indo-Pacific, and Southern oceans within the regions bounded by the continents and the thick white line at 35°S.

the Indian Ocean basin of the Southern Ocean at ∼35°S, as compared with the Atlantic and Pacific basins of the Southern Ocean. However, the bias is equivalent to approximately one contour interval only. The radiocarbon bias is much larger relative to the overall signal (about +31‰ for pure Indian Ocean end-member water) and so we exclude Indian Ocean data when estimating the Southern Ocean remineralization rates shown in Table 1.

[31] In the next section we use the anomaly data from this section to estimate opal dissolution and organic matter remineralization rates, and then we turn to the model study of *Schlitzer* [2004] to examine not only the relative rates for different regions, but also the extent to which the observed differences are due to deep dissolution of opal relative to organic matter remineralization, or to dominance of Southern Ocean opal export.

4. Opal Dissolution and Nitrate Remineralization Rate Estimates

[32] Figure 10 shows scatter plots of ΔSi versus ΔN, and Figure 11 shows each of these plotted versus age, all for data below 2000 m. These data have been used to estimate $\Delta Si/\Delta N$, $\Delta Si/\tau$ and $\Delta N/\tau$ as explained in the footnotes to Table 1. The results are shown in Table 1 along with volume integrals of the rate estimates.

[33] The ΔSi/ΔN slope of the Southern Ocean is 3.1 times the Atlantic, with the Pacific and Indian Ocean slopes falling between these (Table 1). The opal dissolution rate estimates summarized in Table 1 show that three quarters of the dissolution occurs in the Southern Ocean, with the Pacific accounting for 19% of the rest. By contrast, only 56% of the nitrate remineralization occurs in the Southern Ocean, with large additional contributions from the Pacific (25%) and Atlantic (15%) oceans. This reinforces our earlier impressions of the relative importance of the Southern Ocean for opal dissolution over all other basins, with the Pacific playing a secondary role. However, these results show that nitrate also has quite high remineralization rates in the Southern Ocean.

[34] An alternative approach for estimating opal dissolution and organic matter remineralization rates is to combine a wide range of observational constraints on ocean circulation and biogeochemical cycling in an adjoint model such as

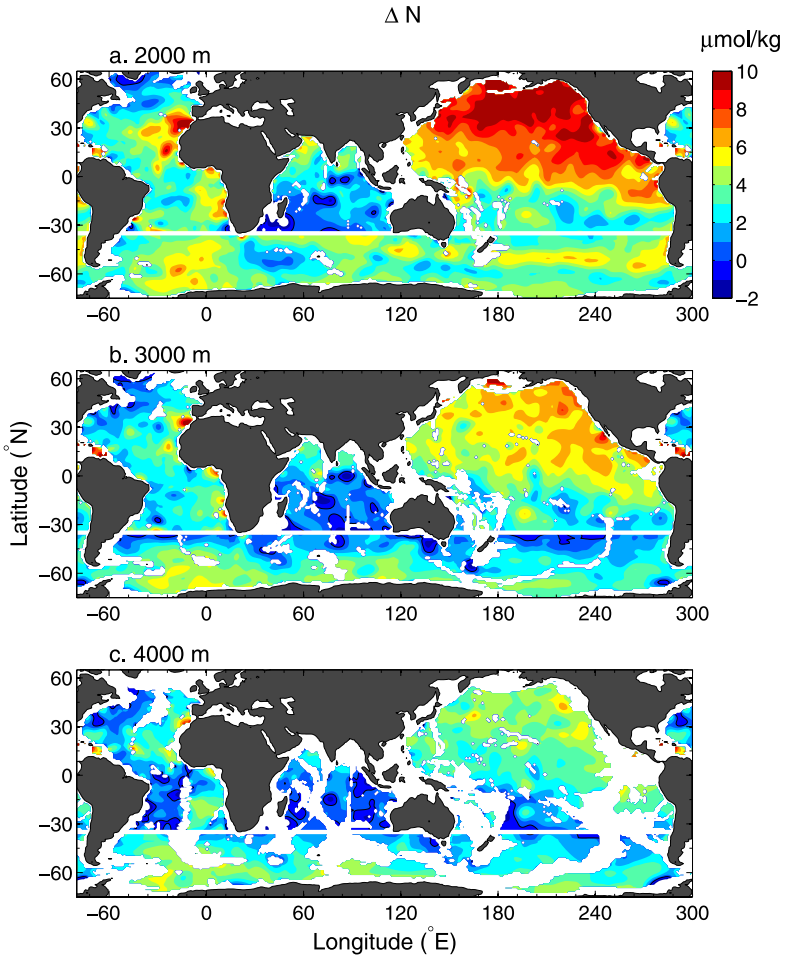

Figure 9. Global maps of ΔN based on the World Ocean Atlas 2001 and GLODAP Atlas [*Conkright et al.*, 2002; *Key et al.*, 2004; *Sabine et al.*, 2005] and analyzed as described in the text. The analysis is performed separately for the Atlantic, Indo-Pacific, and Southern oceans within the regions bounded by the continents and the thick white line at 35°S.

that described by *Schlitzer* [2000]. A new such model has been developed by *Schlitzer* [2006] that includes natural radiocarbon and chlorofluorocarbon observational constraints as well as hydrographic data, nutrients and oxygen. This model has been used to estimate the previously unpublished results summarized in Tables 2 and 3. Details of earlier versions of the biogeochemical component of this adjoint model are described by *Schlitzer* [2000], with further discussion of the results by *Schlitzer* [2002, 2004]. The overall opal flux of 132 Tmol yr^{-1} and the organic carbon flux of 9.4 Pg C yr^{-1} that one obtains from the nitrogen flux using a C:N mole ratio of 117:16 are comparable to a wide range of other estimates in the literature [cf. *Sarmiento and Gruber*, 2006]. An uncertainty of 10–15% is estimated for particulate organic matter export on the basis of sensitivity studies in which the export was minimized and maximized subject to fitting the observations.

[35] A key aspect of the biogeochemical model that is of direct relevance to our discussion here is that the opal and organic matter fluxes are modeled by the function

$$\Phi(z) = \alpha(z/133\ \mathrm{m})^{-b}. \qquad (12)$$

The parameter α is the export production and b is the scaling length of opal dissolution or organic matter remineralization. The depth of 133 m is the base of the euphotic zone in the model. The two parameters α and b are estimated independently for each tracer and each grid box by fitting the observations of silicic acid and nitrate subject to the specified ocean circulation and mixing. This particular version of the model does not include sediments and follows the usual practice in such cases of returning to solution any particulate flux reaching the bottom of the ocean. Hence the dissolution and remineralization occurring below any depth level is equal to the downward flux across that depth level. The effect of including sediments was examined in earlier versions of the adjoint model and was shown to have a negligible impact on the estimated magnitude of export fluxes and water column fluxes and remineralization rates.

[36] The opal flux results in Table 2 show that the Southern Ocean is unique in accounting for 67% of the opal input to the deep ocean below 2000 m, while the Pacific accounts for an additional 23%. The Atlantic and Indian oceans account for only 4.5% and 6.0% of the global opal flux, respectively.

Table 1. Data Below 2000 m, Used to Estimate the Ratio of Opal Dissolution to Organic Nitrogen Remineralization and the Rate of Opal Dissolution and Organic Nitrogen Remineralization for Each Ocean Basin[a]

Property	Units	Atlantic[b]	Southern Ocean[c]	Indian[b]	Pacific[b]	Total
		Ratio of Opal Dissolution to Organic Nitrogen Remineralization				
$\Delta Si/\Delta N$	mol mol^{-1}	2.58 ± 0.28	8.1 ± 1.5	3.98 ± 0.46	6.51 ± 0.30	
(R^2)		(0.44)		(0.34)	(0.62)	
		Average Opal Dissolution and Organic Nitrogen Remineralization Rate				
$\Delta Si/\tau$	μmol kg^{-1} yr^{-1}	0.040 ± 0.006	0.376 ± 0.0.089	0.019 ± 0.006	0.058 ± 0.004	
(R^2)		(0.40)		(0.09)	(0.55)	
$\Delta N/\tau$	μmol kg^{-1} yr^{-1}	0.013 ± 0.002	0.0303 ± 0.0053	0.0048 ± 0.0006	0.0084 ± 0.0003	
(R^2)		(0.69)		(0.28)	(0.75)	
		Volume Integral				
V	$\times 10^{16}$ m^3	11.1	18.4	8.1	30	
$V \cdot \Delta Si/\tau$	$\times 10^{12}$ mol yr^{-1}	4.6	71.1	1.6	17.9	95.1
	(% of total)	(4.8%)	(74.7%)	(1.7%)	(18.8%)	
$V \cdot \Delta N/\tau$	$\times 10^{12}$ mol yr^{-1}	1.5	5.7	0.4	2.6	10.2
	(% of total)	(14.5%)	(56.2%)	(3.9%)	(25.4%)	

[a]See Figure 10 for further details on the ratio of opal dissolution to organic nitrogen remineralization and see Figure 11 for the rates.
[b]Slopes, 95% confidence limits, and R^2 are estimated using a Markov Chain Monte Carlo method based on the Metropolis-Hastings simulated annealing algorithm.
[c]In the Southern Ocean, the clustering of the ΔSi and ΔN versus τ data do not permit fitting a straight line with any confidence, so here we estimated the ratios using the mean of ΔSi, ΔN and τ. In addition, we excluded data from the entire Indian Ocean basin of the Southern Ocean in order to avoid contamination by the end-member bias discussed in the text. The uncertainty is estimated using the bootstrap method with 10,000 trial data sets constructed from the original data set by random selection with replacement. The "best" estimates shown in Table 1 are the median of all the individual estimates, and the 95% confidence limits come directly from the 2.5% and 97.5% tails of the resulting distribution.

These results are in excellent agreement with those given in Table 1 except for the Indian Ocean, which has a low R^2. By contrast, the Southern Ocean organic nitrogen input across 2000 m (Table 3) accounts for only 28% of the global total. The fractional contribution of all the other basins to the organic nitrogen flux is larger than for opal dissolution, including the Pacific Ocean, which accounts for 39% of the total organic matter flux. This smoother distribution of the nitrogen fluxes is closer to what we had predicted we would observe than the results summarized in Table 1, which have a much larger Southern Ocean flux. We have greater confidence in the adjoint model result, which includes a wider array of observations and has a more rigorous approach to fitting the observations.

[37] In order to better understand exactly why the Southern Ocean and Pacific dominate the opal input to the deep ocean in the adjoint model analysis, we separate the 2000 m flux into components as follows:

$$\Phi_i(2000\text{ m}) = \Phi_{Total}(133\text{ m}) \cdot f_i^{133\text{ m}} \cdot f_i^{2000\text{ m}/133\text{ m}}. \quad (13)$$

Here Φ_i(2000 m) is the areally integrated 2000 m flux in basin i. This is a function of the global export production at 133 m, Φ_{Total}(133 m), multiplied by the fraction of this export production that occurs in basin i, $f_i^{133\text{m}}$; and by the preservation fraction, $f_i^{2000\text{m}/133\text{m}}$, i.e., that fraction of the 133 m flux in basin i that survives to a depth of 2000 m without dissolving.

[38] It is instructive to further break down the export production and preservation fractions into a component that represents the expected global average behavior, and another component that represents a local enhancement factor relative to the global mean, which we will symbolize by ε. In the case of the export production fraction within a given basin, $f_i^{133\text{ m}}$, the expected average behavior is that it should equal the fraction of the global area contained within that basin, f_i^{Area}. We thus have

$$f_i^{133\text{ m}} = f_i^{Area} \cdot \varepsilon_i^{production}, \quad (14)$$

where

$$f_i^{Area} = \frac{Area_i}{Area_{Total}}$$
$$\varepsilon_i^{production} = \frac{\Phi_i(133\text{ m})/\Phi_{Total}(133\text{ m})}{f_i^{Area}} \quad (15)$$

In the case of the preservation fraction, the expected behavior is the global average, $f_{Average}^{2000\text{ m}/133\text{ m}}$. We thus have

$$f_i^{2000\text{ m}/133\text{ m}} = f_{Average}^{2000\text{ m}/133\text{ m}} \cdot \varepsilon_i^{preservation}, \quad (16)$$

where

$$f_{Average}^{2000\text{ m}/133\text{ m}} = \frac{\Phi_{Total}(2000\text{ m})}{\Phi_{Total}(133\text{ m})}$$
$$\varepsilon_i^{preservation} = \frac{\Phi_i(2000\text{ m})/\Phi_i(133\text{ m})}{f_{Average}^{2000\text{ m}/133\text{ m}}} \quad (17)$$

Note that the ratios in (17) can be related back to the constant b in the particle flux equation $\Phi(z) = \alpha\,(z/133\text{ m})^{-b}$

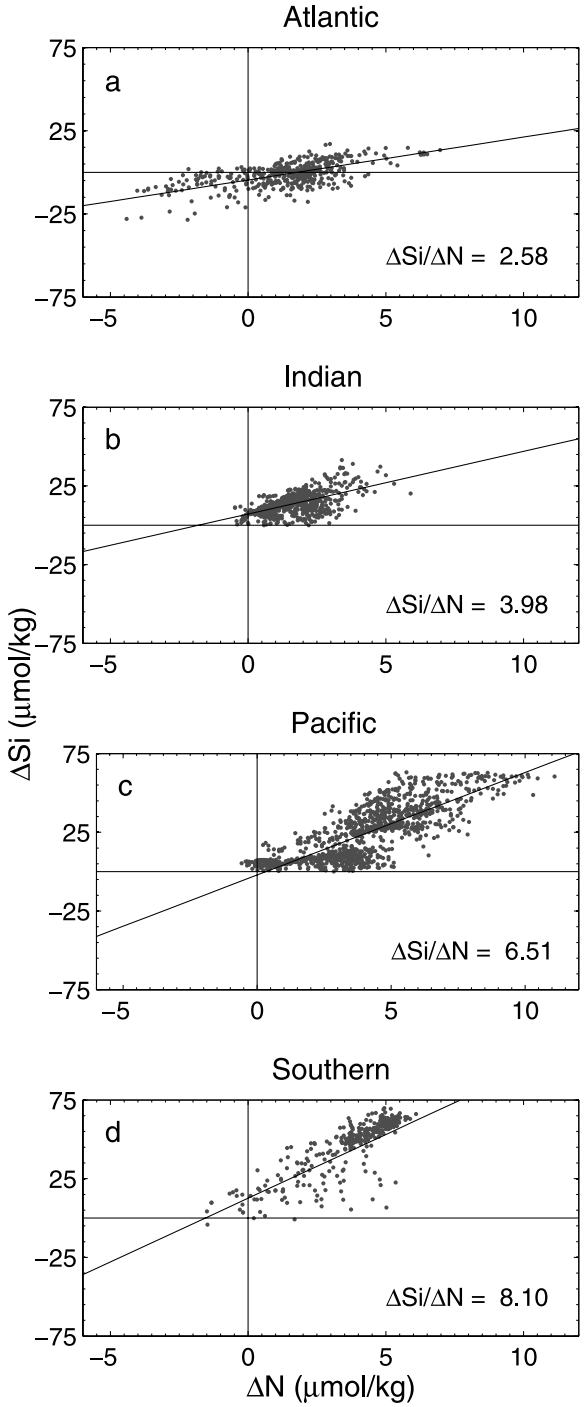

Figure 10. Scatter plots of ΔSi versus ΔN within the (a) Atlantic, (b) Indian, (c) Pacific and (d) Southern oceans. Data shown are from GLODAP discrete samples that have radiocarbon measurements. The slope was estimated as described in the footnotes to Table 1.

used in the adjoint biogeochemical model. Specifically, one can readily show that $\Phi(2000\text{ m})/\Phi(133\text{ m}) = (2000/133)^{-b}$.

[39] Table 2 summarizes our analysis of the opal fluxes by basin. The enhancement factor for the export production shows that the Southern Ocean stands out far above the rest of the basins, with a factor of 2.11 (average behavior would give an enhancement factor of 1.0). By contrast, the Pacific is just over a third of this, the Indian Ocean a quarter of it, and the Atlantic Ocean is one seventh of it. Despite the fact that the Pacific enhancement factor is so much smaller than the Southern Ocean enhancement factor, it is still more than 40% larger than the Indian Ocean enhancement factor, and 2.6 times the Atlantic Ocean's. By contrast, the enhancement factor for opal preservation is only slightly larger in the Southern Ocean than the other basins (1.17 versus 0.76 to 0.80). A possible reason it may be larger is because of the temperature effect on the rate of opal dissolution [cf. *Van Cappellen et al.*, 2002].

[40] Table 3 summarizes our analysis of the organic nitrogen fluxes by basin. Here we see that the enhancement factor for export production is much more evenly distributed than for opal, with the Southern Ocean still being higher than other basins, but only by a factor of 1.9 times for the Atlantic Ocean enhancement factor, and much less for the Indian and Pacific oceans. The enhancement factor for preservation varies somewhat more than for opal, with the Atlantic Ocean having the highest preservation factor, perhaps due to large export events associated with the North Atlantic spring bloom. The combined effect of the export production and preservation fractions gives a basin breakdown of the 2000 m organic nitrogen fluxes that is almost exactly equal to the area fraction (compare % organic N flux at 2000 m with f_i^{Area}), quite unlike the case for opal, where we see that the Southern Ocean 2000 m flux is disproportionately high.

[41] Overall, we conclude that the Southern Ocean does indeed have a disproportionate share of the global opal flux both in absolute amount and also relative to the organic nitrogen flux. The primary reason for this enhanced flux is because of the relative enhancement of the opal export from the surface ocean. This result clearly supports our hypothesis regarding the critical role of the Southern Ocean in the cycling of opal and organic matter in the deep ocean.

[42] The opal production enhancement factor in the Pacific Ocean is also bigger than in the Atlantic and Indian oceans, but only modestly so. The preservation enhancement factor is smaller than in other basins, but not significantly so. We must therefore conclude that the primary reason that the Pacific is so important for the deep budget of silicic acid is because of its large area and the long residence time of the deep water. While there is indeed upwelling and/or mixing of silicic acid into the upper ocean in the Pacific, and it does enhance the production, it is really the Southern Ocean that stands out above all others.

[43] We note in concluding, that the relative magnitude of the Southern Ocean to other regions is extraordinarily sensitive to the models used for a wide range of processes such as opal production and export [*Gnanadesikan*, 1999], uptake of bomb radiocarbon and chlorofluorocarbon [*Matsumoto et al.*, 2004], and uptake of anthropogenic CO_2 [*Mignone et al.*, 2006]. The results in Tables 2 and 3 are based on the state-of-the-art adjoint model of *Schlitzer* [2006], which includes natural radiocarbon and chlorofluorocarbon as constraints. However, it should still be viewed

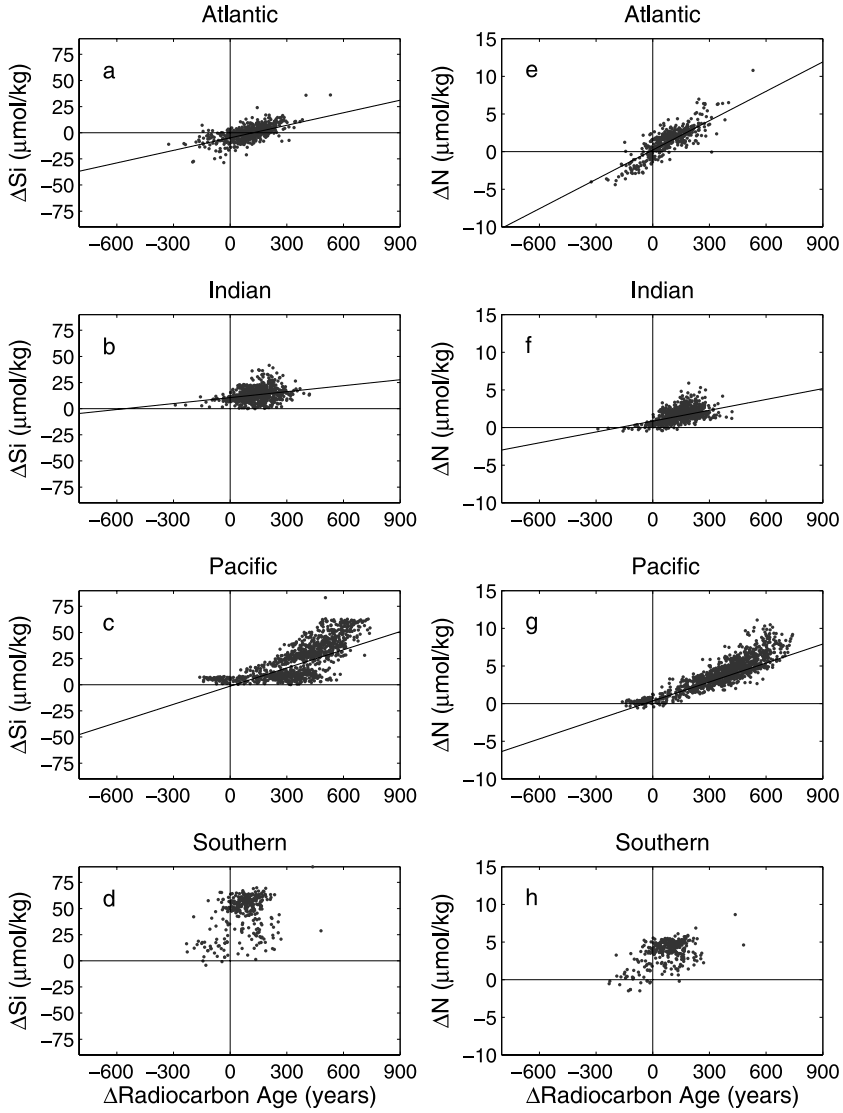

Figure 11. Scatter plots of ΔSi and ΔN versus age estimated from $\Delta(\Delta^{14}C)$. The scatter plots are generated using GLODAP bottle data [*Key et al.*, 2004; *Sabine et al.*, 2005]. Plots are arranged by ocean basin with the Atlantic at the top, then the Indian, Pacific, and Southern oceans. The slopes are estimated as described in the footnotes to Table 1. To ensure the relevant water masses were considered for the slope estimates, data locations associated with $\Delta^{14}C > -100$ ‰ in the Atlantic and silicic acid <115 μmol kg^{-1} in the Indian and Pacific oceans were excluded.

as a step in our evolving understanding of how the global meridional overturning circulation interacts with biogeochemistry to give rise to the observed distribution of tracers.

5. Conclusions

[44] Returning to our conceptual model of Figure 1, what we have shown with our analysis of the observations and quantified with the results shown in Tables 1, 2 and 3, is that a majority of the addition of silicic acid to the deep waters by opal dissolution occurs in the Southern Ocean (67% in the adjoint), with the Pacific accounting for most of the rest (23% in the adjoint). By contrast, the addition of nitrate by organic nitrogen remineralization estimated by the adjoint is much more evenly spread, with the fractional contribution by each basin being almost equal to the fractional area of that basin.

[45] The primary reason for the dominance of the Southern Ocean is the extraordinarily high mole ratio of opal to organic matter export across the base of the euphotic zone in this region [*Sarmiento et al.*, 2004], as well as the high total flux relative to open ocean areas [e.g., *Ragueneau et al.*, 2000; *Sarmiento and Gruber*, 2006]. The high total flux is due to the strong upwelling of nutrient rich waters. The high Si:N ratio of the export flux in the Southern Ocean has been attributed to iron limitation [*Franck et al.*, 2000], but light

Table 2. Opal Flux Estimates Based on the Adjoint Model of *Schlitzer* [2006][a]

Property	Atlantic	Southern Ocean	Indian	Pacific	Total
		Inversion Results (Fluxes in $\times 10^{12}$ mol yr^{-1})			
Opal flux at 133 m, Φ(133 m)	7.4	75.5	9.3	40.1	132.3
Opal flux at 2000 m, Φ(2000 m)[b]	4.2	62.6	5.6	21.6	94.0
	(4.5%)	(66.6%)	(6.0%)	(23.0%)	
		Export Production Fraction			
(a) = f_i^{Area} [c]	0.19	0.27	0.13	0.41	1.00
$\times \varepsilon_i^{production}$	0.29	2.11	0.53	0.75	1.00
= f_i^{133m}	0.06	0.57	0.07	0.30	1.00
		Preservation Fraction			
(b) = $f_{Average}^{2000m/133m}$	0.71	0.71	0.71	0.71	0.71
$\times \varepsilon_i^{preservation}$	0.80	1.17	0.85	0.76	1.00
= $f_i^{2000m/133m}$	0.57	0.83	0.60	0.54	0.71
		Combined Effect of Production and Dissolution Fractions[b]			
(a) × (b)	0.03	0.47	0.04	0.16	0.71
= local flux at 2000 m	(4.5%)	(66.6%)	(6.0%)	(23.0%)	
÷ global flux at 133 m					

[a]See text for definition of terms.
[b]The percent in parentheses is relative to the total given in the far right column.
[c]The fractional breakdown of areas is based on the following areas in units of $\times 10^6$ km^2: Atlantic, 65.44; Southern Ocean, 92.43; Indian, 44.89; Pacific, 138.60; total, 341.36.

limitation as well as other stresses can cause the same phenomenon [cf. *Hutchins and Bruland*, 1998; *Takeda*, 1998; *Martin-Jezequel et al.*, 2000; *Watson et al.*, 2000; *Claquin et al.*, 2002; *Leynaert et al.*, 2004].

[46] Our study is somewhat less clear on the possible role that deep dissolution of opal in the Southern Ocean might play in trapping silicic acid there. What we can say from the sediment trap analysis of *Ragueneau et al.* [2002] and, to a great extent from our own results in Tables 2 and 3, is that the vertical flux profiles of opal and organic matter fluxes in the Southern Ocean do not differ significantly from the rest of the world. However, in order to clearly resolve whether deep opal dissolution is an important mechanism in determining the relative distribution of silicic acid and nitrate in the deep ocean, we would need to run model simulations in which opal and organic matter have "realistic" dissolution profiles, and then a second sensitivity study where the dissolution profiles were identical. We are reasonably confident that both simulations would show a similar relative enhancement pattern of deep silicic acid relative to nitrate because even with shallow dissolution, the efficient stripping out of silicic acid by diatoms would prevent silicic acid from following the same pathway as nitrate out of the

Table 3. Organic Nitrogen Flux Estimates Based on the Adjoint Model of *Schlitzer* [2006][a]

Property	Atlantic	Southern Ocean	Indian	Pacific	Total
		Inversion Results (Fluxes in $\times 10^{12}$ mol yr^{-1})			
Organic N flux at 133 m	15.8	33.8	12.6	44.6	106.8
Organic N flux at 2000 m[b]	1.5	2.1	1.0	2.9	7.5
	(20%)	(28%)	(13%)	(39%)	
		Export Production Fraction			
(a) = f_i^{Area} [c]	0.19	0.27	0.13	0.41	1.00
$\times \varepsilon_i^{production}$	0.78	1.17	0.90	1.03	1.00
= $f_i^{133\ m}$	0.15	0.32	0.12	0.42	1.00
		Preservation Fraction			
(b) = $f_{Average}^{2000\ m/133\ m}$	0.07	0.07	0.07	0.07	0.07
$\times \varepsilon_i^{preservation}$	1.40	0.88	1.13	0.93	1.00
= $f_i^{2000\ m/133\ m}$	0.09	0.06	0.08	0.07	0.07
		Combined Effect of Production and Dissolution Fractions[b]			
(a) × (b)	0.014	0.020	0.009	0.027	0.070
= Local flux at 2000 m	(20%)	(28%)	(13%)	(39%)	
÷ Global flux at 133 m					

[a]See text for definition of terms.
[b]The percent in parentheses is relative to the total given in the far right column.
[c]Area breakdown is as in Table 2.

Southern Ocean into the base of the main thermocline in SAMW as documented by *Sarmiento et al.* [2004].

[47] **Acknowledgments.** The authors wish to thank Cyril Crevoisier, Sara Mikaloff Fletcher, Andy Jacobson, and Steve Pacala for their contributions to the statistical data analysis. N. G. acknowledges support by the Office of Science (BER), U.S. Department of Energy, grant DE-FG03-00ER63010. J. L. S. and J. S. were supported by NSF OCE-0327189. This report was prepared by J. L. S. under award NA17RJ2612 from the National Oceanic and Atmospheric Administration, U.S. Department of Commerce. The statements, findings, conclusions, and recommendations are those of the authors and do not necessarily reflect the views of NOAA, or the U.S. Department of Commerce.

References

Anderson, L. A., and J. L. Sarmiento (1994), Redfield ratios of remineralization determined by nutrient data analysis, *Global Biogeochem. Cycles*, *8*, 65–80.

Brewer, P. G., G. T. F. Wong, M. P. Bacon, and D. W. Spencer (1975), An oceanic calcium problem?, *Earth Planet. Sci. Lett.*, *26*, 81–87.

Broecker, W. S. (1991), The great ocean conveyor, *Oceanography*, *4*, 79–90.

Broecker, W. S., and T.-H. Peng (1982), *Tracers in the Sea*, 690 pp., Lamont-Doherty Geol. Obs., Palisades, New York.

Broecker, W. S., S. Blanton, W. M. Smethie, and G. Ostlund (1991), Radiocarbon decay and oxygen utilization in the deep Atlantic Ocean, *Global Biogeochem. Cycles*, *5*, 87–117.

Brzezinski, M. A. (1985), The Si:C:N ratio of marine diatoms: Interspecific variability and the effect of some environmental variables, *J. Phycol.*, *21*, 347–357.

Claquin, P., V. Martin-Jézéquel, J. C. Kronmkamp, M. J. W. Veldhuis, and G. W. Kraay (2002), Uncoupling of silicon compared with carbon and nitrogen metabolisms and the role of the cell cycle in continuous cultures of *Thalassiosira Pseudonana* (Bacillariophyceae) under light, nitrogen, and phosphorus control, *J. Phycol.*, *38*, 922–930.

Conkright, M. E., et al. (2002), *World Ocean Database 2001*, vol. 1, *Introduction*, 167 pp., U.S. Gov. Print. Off., Washington, D. C.

Franck, V. M., M. A. Brzezinski, K. H. Coale, and D. M. Nelson (2000), Iron and silicic acid concentrations regulate Si uptake north and south of the Polar Frontal Zone in the Pacific Sector of the Southern Ocean, *Deep Sea Res., Part II*, *47*, 3315–3338.

Gnanadesikan, A. (1999), A global model of silicon cycling: Sensitivity to eddy parameterization and dissolution, *Global Biogeochem. Cycles*, *13*, 199–220.

Gnanadesikan, A., J. P. Dunne, R. M. Key, K. Matsumoto, J. L. Sarmiento, R. D. Slater, and P. S. Swathi (2004), Oceanic ventilation and biogeochemical cycling: Understanding the physical mechanisms that produce realistic distributions of tracers and productivity, *Global Biogeochem. Cycles*, *18*, GB4010, doi:10.1029/2003GB002097.

Gnanadesikan, A., et al. (2007), Oceanic ventilation and biogeochemical cycling: Understanding the physical mechanisms that produce realistic distributions of tracers and productivity, *J. Clim.*, in press.

Hallberg, R. W., and A. Gnanadesikan (2007), The role of eddies in determining the structure and response of the wind-driven Southern Hemisphere overturning: Results from the Modeling Eddies in the Southern Ocean Project, *Journal of Physical Oceanography.*.

Hutchins, D. A., and K. W. Bruland (1998), Iron-limited diatom growth and Si:N uptake ratios in a coastal upwelling regime, *Nature*, *393*, 561–564.

Key, R. M., A. Kozyr, C. L. Sabine, K. Lee, R. Wanninkhof, J. Bullister, R. A. Feely, F. Millero, C. W. Mordy, and T.-H. Peng (2004), A global ocean carbon climatology: Results from Global Data Analysis Project (GLODAP), *Global Biogeochem. Cycles*, *18*, GB4031, doi:10.1029/2004GB002247.

Ledwell, J. R., A. J. Watson, and C. S. Law (1993), Evidence for slow mixing across the pycnocline from an open-ocean tracer-release experiment, *Nature*, *364*, 701–703.

Leynaert, A., E. Bucciarelli, P. Claquin, R. C. Dugdale, V. Martin-Jézéquel, P. Pondaven, and O. Ragueneau (2004), Effect of iron deficiency on diatom cell size and silicic acid uptake kinetics, *Limnol. Oceanogr.*, *49*, 1134–1143.

Mantyla, A. W., and J. L. Reid (1995), On the origins of deep and bottom waters of the Indian Ocean, *J. Geophys. Res.*, *100*, 2417–2439.

Marinov, I., A. Gnanadesikan, J. R. Toggweiler, and J. L. Sarmiento (2006), The Southern Ocean biogeochemical divide, *Nature*, *441*, 964–967.

Martin-Jezequel, V., M. Hildebrand, and M. A. Brzezinski (2000), Silicon metabolism in diatoms: Implications for growth, *J. Phycol.*, *36*, 821–840.

Matsumoto, K., et al. (2004), Evaluation of ocean carbon models with data-based metrics, *Geophys. Res. Lett.*, *31*, L07303, doi:10.1029/2003GL018970.

Mignone, B. K., A. Gnanadesikan, J. L. Sarmiento, and R. D. Slater (2006), Central role of Southern Hemisphere winds and eddies in modulating the oceanic uptake of anthropogenic carbon, *Geophys. Res. Lett.*, *33*, L01604, doi:10.1029/2005GL024464.

Ragueneau, O., et al. (2000), A review of the Si cycle in the modern ocean: Recent progress and missing gaps in the application of biogenic opal as a paleoproductivity proxy, *Global Planet. Change*, *26*, 317–365.

Ragueneau, O., N. Dittert, P. Pondaven, P. Treguer, and L. Corrin (2002), Si/C decoupling in the world ocean: Is the Southern Ocean different?, *Deep Sea Res., Part II*, *49*, 3127–3154.

Reid, J. L. (1997), On the total geostrophic circulation of the Pacific Ocean: Flow patterns, tracers, and transport, *Prog. Oceanogr.*, *29*, 263–352.

Sabine, C. L., R. M. Key, A. Kozyr, R. A. Feely, R. Wannninkhof, F. J. Millero, T.-H. Peng, J. L. Bullister, and K. Lee (2005), Global Ocean Data Analysis Project: Results and data, *ORNL/CDIAC-145, NDP-083*, 110 pp., Carbon Dioxide Inf. Anal. Cent., Oak Ridge Natl. Lab., U.S. Dep. of Energy, Oak Ridge, Tenn.

Sarmiento, J. L., and N. Gruber (2006), *Ocean Biogeochemical Dynamics*, Princeton Univ. Press, Princeton, N. J.

Sarmiento, J. L., J. Dunne, A. Gnanadesikan, R. M. Key, K. Matsumoto, and R. Slater (2002), A new estimate of the $CaCO_3$ to organic carbon export ratio, *Global Biogeochem. Cycles*, *16*(4), 1107, doi:10.1029/2002GB001919.

Sarmiento, J. L., N. Gruber, M. A. Brzezinski, and J. P. Dunne (2004), High latitude controls of thermocline nutrients and low latitude biological productivity, *Nature*, *427*, 56–60.

Schlitzer, R. (2000), Applying the adjoint method for biogeochemical modelling, in *Inverse Methods in Global Biogeochemical Cycles*, *Geophys. Monogr. Ser.*, vol. 114, edited by P. Khasibhatla et al., pp. 107–124, AGU, Washington, D. C.

Schlitzer, R. (2002), Carbon export fluxes in the Southern Ocean: Results from inverse modeling and comparison with satellite-based estimates, *Deep Sea Res., Part II*, *49*, 1623–1644.

Schlitzer, R. (2004), Export production in the equatorial and North Pacific derived from dissolved oxygen, nutrient, and carbon data, *J. Oceanogr.*, *60*, 53–62.

Schlitzer, R. (2006), Assimilation of radiocarbon and chlorofluorocarbon data to constrain deep and bottom water transports in the world ocean, *J. Phys. Oceanogr.*

Sloyan, B. M., and S. R. Rintoul (2001), Circulation, renewal, and modification of Antarctic Mode and Intermediate Water, *J. Phys. Oceanogr.*, *31*, 1005–1030.

Takeda, S. (1998), Influence of iron availability on nutrient consumption ratio of diatoms in oceanic waters, *Nature*, *393*, 774–777.

Talley, L. D., J. L. Reid, and P. E. Robbins (2003), Data-based meridional overturning streamfunctions for the global ocean, *J. Clim.*, *16*, 3213–3226.

Van Cappellen, P., S. Dixit, and J. van Beusekom (2002), Biogenic silica dissolution in the oceans: Reconciling experimental and field-based dissolution rates, *Global Biogeochem. Cycles*, *16*(4), 1075, doi:10.1029/2001GB001431.

Watson, A. J., D. C. E. Bakker, A. J. Ridgwell, P. W. Boyd, and C. S. Law (2000), Effect of iron supply on Southern Ocean CO_2 uptake and implications for glacial atmospheric CO_2, *Nature*, *407*, 730–733.

A. Gnanadesikan, Geophysical Fluid Dynamics Laboratory, P.O. Box 308, Princeton, NJ 08542, USA. (anand.gnanadesikan@noaa.gov)

N. Gruber, Institute of Biogeochemistry and Pollutant Dynamics, ETH Zurich, CHN E21.1, CH-8092 Zurich, Switzerland. (nicolas.gurber@env.ethz.ch)

R. M. Key, J. L. Sarmiento, and J. Simeon, Program in Atmospheric and Ocean Sciences, Princeton University, P.O. Box CN710, Princeton, NJ 08544-0710, USA. (key@princeton.edu; jls@princeton.edu; jsimeon@princeton.edu)

R. Schlitzer, Alfred-Wegener-Institute, Am Handelshafen 12, Columbusstrasse, D-27568 Bremerhaven, Germany. (reiner.schlitzer@awi.de)